IRE1 Signaling Is Essential for Ischemia-Induced Vascular Endothelial Growth Factor-A Expression and Contributes to Angiogenesis and Tumor Growth *In vivo*

Benjamin Drogat,[1,2] Patrick Auguste,[1,3,6] Duc Thang Nguyen,[3] Marion Bouchecareilh,[1,2,3,6,7] Raphael Pineau,[1,2] Josephine Nalbantoglu,[4] Randal J. Kaufman,[5] Eric Chevet,[3,6,7] Andréas Bikfalvi,[1,2] and Michel Moenner[1,2]

[1]Inserm, E0113; [2]Université Bordeaux 1, Talence, France; [3]Organelle Signaling Laboratory, Departments of Surgery and [4]Neurology and Neurosurgery, McGill University, Montreal, Quebec, Canada; [5]Howard Hughes Medical Institute, Departments of Biological Chemistry and Internal Medicine, University of Michigan Medical Center, Ann Arbor, Michigan; [6]Inserm, U889, Team Avenir; and [7]Université Bordeaux 2, Bordeaux, France

Abstract

In solid tumors, cancer cells subjected to ischemic conditions trigger distinct signaling pathways contributing to angiogenic stimulation and tumor development. Characteristic features of tumor ischemia include hypoxia and glucose deprivation, leading to the activation of hypoxia-inducible factor-1–dependent signaling pathways and to complex signaling events known as the unfolded protein response. Here, we show that the activation of the endoplasmic reticulum stress sensor IRE1 is a common determinant linking hypoxia- and hypoglycemia-dependent responses to the up-regulation of vascular endothelial growth factor-A (VEGF-A). Tumor cells expressing a dominant-negative IRE1 transgene as well as *Ire1*α-null mouse embryonic fibroblasts were unable to trigger VEGF-A up-regulation upon either oxygen or glucose deprivation. These data correlated with a reduction of tumor angiogenesis and growth *in vivo*. Our results therefore suggest an essential role for IRE1-dependent signaling pathways in response to ischemia and identify this protein as a potential therapeutic target to control both the angiogenic switch and tumor development. [Cancer Res 2007;67(14):6700–7]

Introduction

Solid tumors initially develop in the absence of vascularization and are subjected to various growth constraints due to ischemia. Among those, the decrease in oxygen pressure in tissues induces a pleiotropic cellular response that includes metabolic adaptation, apoptosis, and angiogenesis, mainly through stabilization and intracellular accumulation of the hypoxia-inducing transcription factor hypoxia-inducible factor-1α (HIF-1α; ref. 1). Alternatively, limited glucose supply triggers a complex and diversified primary response that includes ATP depletion (2), expression of proteins and lipids exhibiting altered glycosylation profiles (3), and release of reactive oxygen species (4). These, in turn, have different metabolic consequences in the control of cellular redox potential, protein trafficking, and, more generally, in tumor cell survival and aggressiveness (4–6). Both glucose deprivation and hypoxia activate a characteristic stress signaling pathway in the endoplasmic reticulum (ER) named the unfolded protein response (UPR; ref. 6). The significance of the UPR in mammals has been reported in several physiologic and pathophysiologic situations (5, 7).

The UPR consists of a translational attenuation process combined with the transcriptional activation of specific target genes coding for regulatory proteins including resident molecular chaperones. These events are under the control of three major ER resident integral membrane proteins, namely the PRK-like ER kinase (PERK), the activating transcription factor-6, and the inositol-requiring enzymes 1 (IRE1α and IRE1β isoforms; ref. 7). Upon ER stress, PERK activation promotes the rapid phosphorylation of the translation initiation factor eIF2α (8) that in turn leads to translation attenuation. Moreover, PERK activation has been linked to translation inhibition under hypoxic stress (9) and involved in the regulation of tumor cell survival (10, 11). IRE1 proteins possess both intrinsic protein kinase and endoribonuclease activities in their cytosolic domain. Upon ER stress, IRE1-containing RNase activity splices an unconventional intron in the X-box–binding protein 1 (XBP1) mRNA, which leads to a frameshift resulting in the translation of a stable transcription factor involved in the transcriptional activation of ER regulatory proteins coding genes such as *EDEM* (12). Recently, XBP1 has been shown to be essential to the survival of transformed cells in response to hypoxia (13).

Vascular endothelial growth factor-A (VEGF-A) is a proangiogenic protein essential for vasculogenesis and normal angiogenesis and is also a key determinant of tumor neovascularization (14). Physiologic stresses inflicted to tumors under ischemic conditions, such as hypoxia (15), nutrient deprivations (15–17), or reactive oxygen species increase (18), induce VEGF-A expression as part of the tumor response to ischemia and therefore may contribute to tumor vascularization and development. However, it is not clear whether the respective intracellular signaling pathways triggered in response to these stresses share any common metabolic determinants, therefore impeding the research of multivalent therapeutic agents. For instance, although hypoxia mediates VEGF-A expression through HIF-1–dependent transcriptional activation (19, 20), the up-regulation of VEGF-A in response to glucose deprivation was found to be HIF-1 independent in several (17, 21, 22), but not all (23–25), cellular models. An increase of VEGF-A transcript stability has also been reported under both stress conditions in tumor cells (15, 17). Thus far, except for the reported role of the AMP-dependent protein kinase (17), the

Note: Supplementary data for this article are available at Cancer Research Online (http://cancerres.aacrjournals.org/).

P. Auguste, D.T. Nguyen, and M. Bouchecareilh contributed equally to this work.

Requests for reprints: Michel Moenner, Inserm E0113, Université Bordeaux 1, Bat B2, Avenue des Facultes, Talence F-33400, France. Phone: 33-540-008-925; Fax: 33-540-00-87-05; E-mail: m.moenner@angio.u-bordeaux1.fr and Eric Chevet, Inserm, U889, Team Avenir, Université Bordeaux 2, 146 rue Leo Saignat, 33076 Bordeaux, France. Phone: 33-557-571-707; E-mail: eric.chevet@u-bordeaux2.fr.

doi:10.1158/0008-5472.CAN-06-3235

intracellular molecular events leading to VEGF-A up-regulation in response to glucose deprivation remain poorly characterized.

Considering that both hypoxia and glucose deprivation activate the UPR, and because VEGF-A is also a transcriptional target of ER stressors such as tunicamycin or thapsigargin (16), we investigated whether the UPR could represent a critical mediator of the regulation of VEGF-A expression in tumor development. We show that the ER proximal signaling molecule IRE1 is a key regulator of VEGF-A expression upon hypoxia and hypoglycemia in three different tumor cell lines and in mouse embryonic fibroblasts. In addition, we show that IRE1 contributes to tumor growth and angiogenesis *in vivo*. We propose a model in which IRE1 may represent a ubiquitous signaling component of tumor cell growth and plasticity.

Experimental Procedures

Reagents. Culture media were from Invitrogen. DMEM without glucose (DMEM F405) was from Merck Eurolab. Serum-free medium containing high-density lipoproteins was used as previously described (26). Tunicamycin was purchased from Sigma. Desmin mouse monoclonal antibodies were from DAKO SA. Goat and rabbit antibodies against human VEGF-A were from Santa Cruz Biotechnology. Primers (Supplementary Table S1) were purchased either from Proligo or Alpha DNA. Oligo(dT)15 was from Invitrogen.

Cell culture. A549/8 human lung carcinoma cells were grown in DMEM/F-12 medium supplemented with 10% fetal bovine serum (FBS), L-glutamine, and antibiotics. U87 and C6 glioma cells were grown in DMEM, 1 g/L glucose supplemented with 10% FBS, L-glutamine, and antibiotics. A549/8 and U87 cells were stably transfected with pcDNA3/IRE1α.NCK-1, an expression vector encoding a cytoplasmic-defective IRE1 mutant (27). Rat C6 cells were stably transfected with the pED-IRE1.K599A plasmid encoding a kinase-defective IRE1 mutant (28). Transfections were done using LipofectAMINE (Invitrogen) according to the manufacturer's recommendations. A549/8 and U87 cells were selected using 1 mg/mL and 450 μg/mL G418, respectively, and C6 cells using 250 μg/mL methotrexate. Three to six independent clones were isolated and characterized for each cell line. Primary wild-type and IRE1α$^{-/-}$ mouse embryonic fibroblasts (MEF) were prepared from embryos from germ line–targeted SV129/J mice that were crossed with C57Bl/6 mice as described (29). Experiments using A549/8 cells and MEFs were carried out in serum-free culture conditions (26). Experiments using U87 cells and C6 cells were carried out in DMEM containing 1% FBS. Experiments in hypoxic conditions were done at 3% O_2 in a Heraeus incubator BB-6060. Glucose deprivation was carried out in A549/8 cells and in MEFs as follows: after a 4-day incubation in serum-free culture conditions, cells were washed and incubated for 15 min in DMEM F405 at 37°C. Cells were then incubated for the indicated periods of time with DMEM F405 supplemented with 25 μg/mL high-density lipoprotein, 5 μg/mL transferrin, 1 mg/mL bovine serum albumin (BSA), 2 mmol/L glutamine, and increasing concentrations of glucose. U87 and C6 cells were subjected to glucose deprivation using DMEM F405 medium supplemented with 1% FBS.

VEGF-A ELISA. Subconfluent cells were grown in 10-cm-diameter dishes for 16 h (U87 cells) or for 24 h (A549/8 cells) under the indicated culture conditions. VEGF-A concentration was measured in conditioned medium using a commercial VEGF ELISA kit (R&D Systems). The assays were done in triplicate and calibration curves were obtained using human recombinant VEGF-A. Results were obtained from at least two independent cultures and were analyzed using the Softmax Pro4.0 software (Molecular Devices Corporation).

Reverse transcription-PCR analyses. Semiquantitative analyses were carried out as previously described (27). Quantitative RT-PCR analyses were done using the MX3000p thermocycler (Stratagene) and the SYBRgreen dye (ABgene) methodology. The relative abundance of transcripts was calculated by using β-actin transcript quantity as standard. The quantitative RT-PCR experiments were carried out in tetraplicate on RNA isolated from two or three independent cell cultures. Homogeneity of PCR products was controlled by melting point analyses and gel electrophoresis.

Immunoblot analyses. Subconfluent cells grown in 10-cm^2 diameter dishes were lysed at 4°C with 20 mmol/L Tris-HCl, 150 mmol/L, NaCl, 1.5% CHAPS, protease inhibitors (P8340; Sigma), 1 mmol/L sodium deoxycholate, 5 mmol/L sodium fluoride (pH 8.0; lysis buffer). Protein content was determined using the BCA protein assay kit (Pierce) and BSA as standard. Fifty to 100 μg of proteins were resolved by SDS-PAGE. After migration, proteins were transferred to a nitrocellulose membrane (Amersham) and probed using antibodies against human VEGF-A and β-actin (Santa Cruz Biotechnology), HIF-1α (BD Biosciences), and HIF-2α (Calbiochem). Proteins were detected using a secondary antibody coupled to horseradish peroxidase (HRP; DAKO SA) and revealed using the ECL reagent (Amersham) followed by radioautography.

Soft-agar colony-forming assay. IRE1 dominant negative (DN)–expressing cells or control cells (20,000) were plated onto six-well plates in DMEM containing 10% FBS and 0.2% agar (overlay) onto the top of an agar underlay (DMEM containing 10% FBS and 0.4% agar). Cells were fed after 5 days with 1.5 mL of overlay, and the colonies were counted after 10 days of incubation under a light microscope at ×20 magnification. Twenty different fields were scored from each well by two independent investigators. Assays were carried out in duplicate and the results were expressed as mean ± SD.

Chorio-allantoic membrane assay. Fertilized chicken eggs were obtained and treated essentially as previously described (30). Five millions A549/8 cells in 20 μL of DMEM were deposited on the surface of the chorio-allantoic membrane (CAM). Tumor progression was then observed daily under a Nikon SMZ stereomicroscope. At days 3, 5, and 7, tumors were removed and mRNAs were extracted. Alternatively, tumors were cut into 10-μm-thick cryosections and stained with H&E for histologic analyses and observation of the tumor vascularization. Pericytes were detected by using mouse antibodies directed against desmin. Experiments were done at least in tetraplicate.

Intracranial injections, tumor size, and blood capillary measurements. Two independent sets of experiments were carried out using either athymic nude mice or Rag γ mice. The protocol used was as previously described (31). Cell implantations were at 2 mm lateral to the bregma and 3 mm in depth using two different sets of clones for both U87 pcDNA3 cells and U87 IRE1.NCK DN cells. Twenty-eight or 30 days postinjection, brain sections were stained using H&E for visualization of tumor masses. Tumor volume was then estimated by measuring the length (L) and width (W) of each tumor and was calculated using the following formula ($L \times W^2 \times 0.5$). CD31-positive vessels were numerated after immunohistologic staining of the vascular bed using rat antibodies against CD31 (PharMingen) and secondary antibodies coupled to HRP (DAKO). Imaging was carried out using a Nikon E600 microscope equipped with a digital camera DMX1200. Blood vessels were quantified by two independent investigators. Capillary

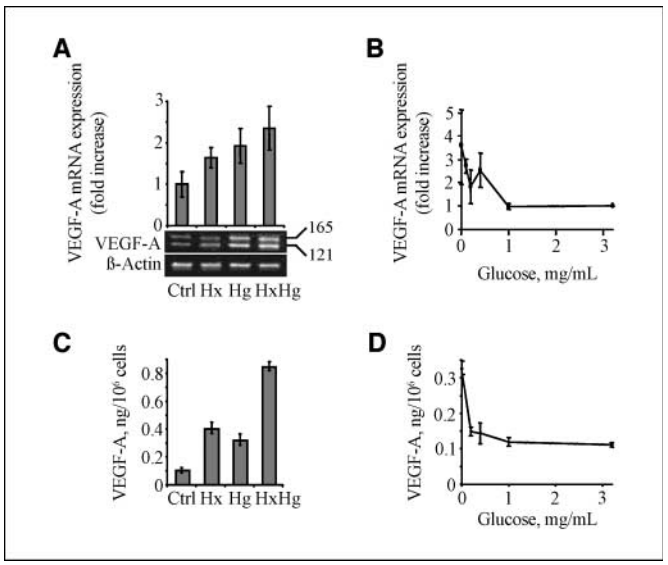

Figure 1. The effect of hypoxia and glucose deprivation on the expression of VEGF-A by A549/8 cells. Cells were grown up to subconfluence in 25-cm^2 culture flasks in serum-free medium. They were then washed and incubated in normoxic (*Ctrl, Hg*; 21% O_2) or in hypoxic (*Hx*; 3% O_2) conditions in the same medium without EGF and insulin, and in the presence (*Ctrl, Hx*) or absence (*Hg*) of 3.2 g/L glucose. Following a 24-h incubation, conditioned medium were collected and total mRNA was isolated. *A,* expression of VEGF-A and β-actin mRNA was measured by semiquantitative reverse transcription-PCR after electrophoresis in a 2% agarose gel. Histogram values represent the sum of the intensities of $VEGF_{121}$ and $VEGF_{165}$ mRNAs. *Columns,* mean of triplicate assays; *bars,* SD. A representative gel electrophoresis pattern is shown under the histogram. *B,* expression of VEGF mRNA in cells exposed to various concentrations of glucose, as determined by real-time quantitative RT-PCR. Indicated values represent the sum of the expression of $VEGF_{121}$ and $VEGF_{165}$ transcripts. Results were normalized using β-actin and were representative of three independent cultures. *C,* quantification of VEGF-A protein accumulation ($VEGF_{121}$ and $VEGF_{165}$ isoforms) by ELISA. *D,* ELISA-based determination of the effect of glucose concentration on the production of VEGF-A. *Points,* mean results obtained from triplicate culture cells; ELISA was done in duplicate or triplicate; *bars,* SD for each determination.

number per square millimeter was then reported after counting of 16 to 68 different fields originating from 8 to 12 independent tumors for each (pcDNA3 and IRE1 DN) condition.

Results

VEGF-A expression upon hypoxia and glucose deprivation in A549/8 cells. The expression of VEGF-A mRNA and protein was measured in A549/8 cells subjected to hypoxia, to glucose deprivation, or to a combination of both stresses for 24 h. VEGF-A mRNA was constitutively expressed in these cells and two transcripts encoding the $VEGF_{121}$ and $VEGF_{165}$ protein products were detected (Fig. 1*A*). Both hypoxia and hypoglycemia usually led to a 1.5- to 3-fold increase in VEGF-A mRNA expression. Dose-response experiments showed that VEGF-A mRNA increased at glucose concentrations equal or lower than 0.4 g/L (Fig. 1*B*). The expression of VEGF-A protein in A549/8 cells was also analyzed using ELISA. Under basal culture conditions, ~0.1 ng VEGF-A were secreted per million cells and per day. Hypoxia or glucose deprivation consistently increased the amount of the growth factor in the medium (~4-fold and 3-fold increases, respectively; Fig. 1*C*). The effect of glucose deprivation on VEGF-A protein expression was dose dependent with maximum secretion observed in the complete absence of glucose (Fig. 1*D*). Thus, hypoxia and glucose deprivation both induce VEGF-A up-regulation at the mRNA and protein levels. Interestingly, this increase was further enhanced when a combination of the two stresses was applied to the cells, suggesting cumulative or synergistic effects (Fig. 1*A* and *C*).

Qualitatively, $VEGF_{165}$ secreted by cells subjected to glucose deprivation, but not to hypoxia, presented an altered mobility by gel electrophoresis with apparent molecular weight lower than expected (38 kDa versus 42 kDa; Supplementary Fig. S2*A*). Although the absence of glucose led to the expression of a structurally different (unglycosylated) VEGF-A, we showed that the growth factor retained full biological activity (Supplementary Fig. S2*B*). These results therefore suggest that low glucose concentration in tumors may indeed generate a potent angiogenic stimulus through increased expression of the fully active 38-kDa VEGF.

Hypoxia- and/or glucose deprivation–activated signaling pathways in A549/8 cells. Because VEGF-A mRNA was up-regulated upon both hypoxia and glucose deprivation in A549/8 cells, we next investigated the potential signaling pathways involved in this process. The expression of HIF-1α and HIF-2α was detected in cells subjected to hypoxia but not in cells subjected to glucose deprivation (Fig. 2*A*). The mRNA expression profile of *GLUT-1, HK-2*, and *PFKFB3* genes whose transcriptional up-regulation under hypoxia is HIF-1α dependent (21, 32), was also determined (Fig. 2*B*). Consistent with the accumulation of HIF-1α, an increase in the expression level of the three mRNAs was observed in cells subjected to hypoxia and, as expected (33), only GLUT-1 mRNA was up-regulated under glucose deprivation. These data indicate that in A549/8 cells, the accumulation of VEGF-A mRNA correlated with the stabilization of HIF proteins under hypoxic conditions but not under glucose deprivation. Finally, VEGF promoter–driven luciferase activity was measured in cells subjected to both stresses (Supplementary Fig. S3). The activity was 2-fold higher under hypoxia than in control conditions after a 24-h incubation. In contrast, no increase was observed in A549/8 cells incubated in the absence of glucose. Therefore, as reported for other cell types (17, 22, 34), the structure of the VEGF-A promoter was not sufficient to explain the increase of VEGF mRNAs in A549/8 cells subjected to glucose deprivation, thus suggesting another mechanism such as mRNA stabilization (17, 34). Together, these results indicate that hypoxia and glucose deprivation might both lead to the up-regulation of VEGF-A through the activation of nonredundant signaling pathways.

An alternative mechanism for VEGF-A mRNA up-regulation under low glucose may come from the activation of the UPR. Indeed, the absence of glucose is a well-documented UPR inducer in various cell models (35) and *VEGF-A* is a target gene of well-known ER stressors such as tunicamycin or thapsigargin (16). In A549/8 cells, the expression of four UPR target genes (*BiP, EDEM, GADD34*, and *CHOP*) was up-regulated upon glucose deprivation (Fig. 2*C*). Although the expression of these genes was not affected upon moderate hypoxia (3% O_2) alone, the combination of both stresses led to a further increase in the expression level of EDEM and GADD34 mRNAs, suggesting the existence of synergistic signaling pathways. The increased expression of EDEM mRNA was further confirmed by the nonconventional splicing of XBP1 mRNA (Fig. 2*D*) detected only in the absence of glucose and upon the combination of both stresses. Therefore, the intracellular responses to moderate hypoxia and to glucose deprivation are apparently well discriminated in A549/8 cells. Severe hypoxia (0.1% O_2), however, also led to XBP1 mRNA splicing and triggering of the UPR (26). Overall, these results show that the observed increase in VEGF-A mRNA under low glucose concentrations correlates with UPR activation, thus suggesting that the two events may be linked.

IRE1-mediated expression of VEGF-A. In an attempt to show a direct link between the activation of the UPR and VEGF-A expression upon glucose deprivation, A549/8 carcinoma cells and U87 glioma cells were transfected with a DN IRE1 construct (IRE1.NCK; ref. 27). Several independent stably transfected clones (at least three of each) were then analyzed for transgene expression and inhibition of XBP1 mRNA splicing (Supplementary Fig. S4*A*). According to the cell type and clone considered, XBP1 splicing inhibition ranges from 64% to 92%. Clones of A549/8 and U87 cells were then subjected to hypoxia or glucose deprivation and the expression of VEGF-A mRNA was monitored (Fig. 3*A–B*). Although VEGF-A transcripts were increased upon hypoxia or in the absence of glucose in cells transfected with the empty vector, their expression remained at a near-basal level in IRE1 DN–expressing cells. Lower levels of expression were also significantly obtained at the protein level (Fig. 3*C–D*), thus indicating that in A549/8 and U87 cells, hypoxia and glucose deprivation increase VEGF-A mRNA in an IRE1-dependent manner. More specifically, these results suggest that IRE1 activation is an essential event that may occur upstream of HIF-1α. In keeping with this hypothesis, HIF-1α expression was shown to decrease at both mRNA and protein levels in IRE1 DN cells compared with pCDNA3 cells (Supplementary Fig. S9). Other cell types were then tested for VEGF-A expression under the dependence of IRE1 activity. To this end, rat C6 glioma cells were stably transfected with expression plasmids containing IRE1.K599A (kinase dead cytoplasmic domain; ref. 28; see Supplementary Fig. S4*A* for transgene expression and XBP1 splicing). These cells were then subjected to hypoxia or to glucose deprivation and the expression of VEGF-A mRNA was monitored (Supplementary Fig. S5*A*). Again, the expression of IRE1 DN activity prevented VEGF-A mRNA up-regulation under both hypoxia and hypoglycemia. Finally, we examined the expression of VEGF mRNA upon similar stress conditions in *IRE1α* ($^{-/-}$) MEFs and in wild-type MEFs. As expected, VEGF-A mRNA had a higher basal expression level in wild-type cells than in mutant cells (Supplementary Fig. S5*B*). In addition, both hypoxia and glucose deprivation led to a significant up-regulation of VEGF transcripts in wild-type MEFs but not in *IRE1α* ($^{-/-}$) MEFs, thus confirming the essential role of IRE1 signaling in the regulation of VEGF-A expression under hypoxia or in the absence of glucose.

IRE1-dependent angiogenesis and tumor growth *in vivo*. Because IRE1 DN–expressing tumor cells exhibit a significantly reduced expression of VEGF-A under hypoxia and under glucose deprivation, we investigated the potential implication of IRE1 activity on the development of solid tumors in two *in vivo* systems. At first, the chicken CAM model (30) was used to study the angiogenic status of A549/8 cell–derived tumors (Fig. 4). The rationale for these experiments was to tentatively favor the nutrient-triggered

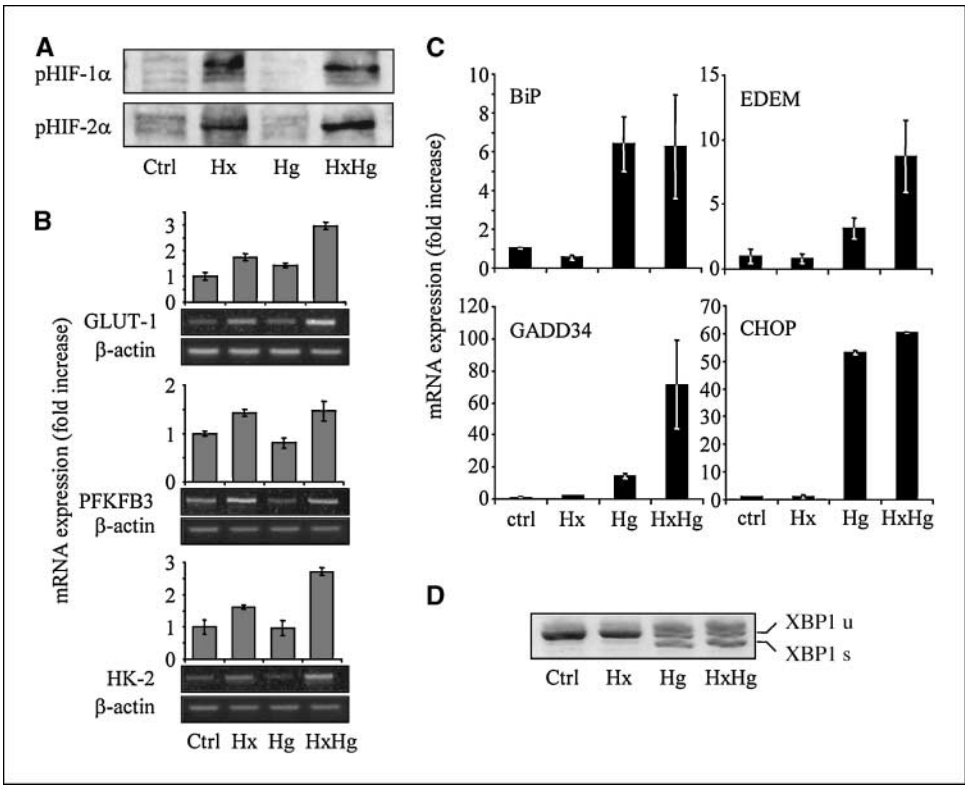

Figure 2. Hypoxia- and/or hypoglycemia-induced signaling pathways in A549/8 cells. A549/8 cells were subjected to hypoxia (*Hx*), hypoglycemia (*Hg*), or to both stresses (*HxHg*) as reported in Fig. 1. *A,* cells were stressed for 6 h and the presence of HIF-1α and HIF-2α was examined by immunoblot using anti–HIF-1α (*pHIF-1α*) and anti–HIF-2α (*pHIF-2α*) antibodies. One hundred micrograms of total proteins were loaded in each well and β-actin was used as the internal control. Experiment was repeated twice with similar results. *B,* RT-PCR analyses of mRNA expression of GLUT-1, HK-2, and PFKFB3. Cells were stressed for 24 h and mRNA levels were determined. *Columns,* mean of triplicate experiments; *bars,* SD. Representative of three independent cell cultures. *C,* quantitative RT-PCR analysis of UPR-dependent gene expression. Gene expression ratio of each target gene to β-actin is presented after a 24-h incubation under various stress conditions as fold induction relative to control conditions. *Columns,* mean of triplicate experiments; *bars,* SD. Measures were done on two or three independent cultures. *D,* XBP1 mRNA splicing by IRE1 was analyzed by RT-PCR. Cells were exposed to hypoxia or/and to glucose deprivation for 4 h. PCR analyses were done using primers flanking the XBP1 mRNA splicing site. *XBP1u,* unspliced form of the transcripts; *XBP1s,* spliced form of the transcripts. PCR products were resolved by electrophoresis on a 3% agarose gel and stained with ethidium bromide before observation.

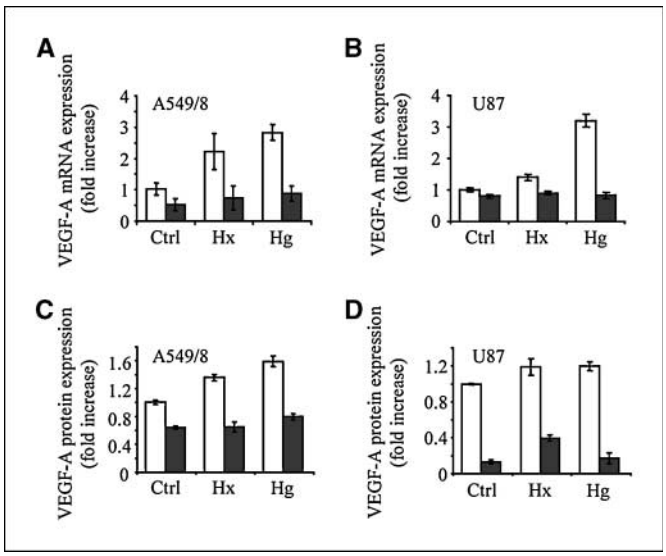

Figure 3. Hypoxia- or hypoglycemia-induced VEGF-A expression is dependent on IRE1 signaling. A549/8 and U87 cells were stably transfected with empty or DN vectors and individual clones were selected on the basis of high levels of IRE1 DN expression and inhibition of XBP1 mRNA splicing (Supplementary Fig. S4*A*). Cells were then incubated for 16 h (U87) or 24 h (A549/8) in normal culture conditions (*Ctrl*) or under hypoxia (*Hx*) or glucose deprivation (*Hg*). VEGF-A expression in DN mutant of IRE1 (IRE1.NCK, *closed columns*) was compared with that observed in cells expressing the empty vector (pCDNA3, *open columns*). VEGF-A mRNA expression was measured by RT-PCR. The ratios of VEGF-A expression to β-actin expression are presented as fold increase relative to control conditions obtained with pcDNA3 cells. VEGF-A protein expression was quantified by ELISA. Representative results. *A,* VEGF-A mRNA expression in A549/8 cells; *B,* VEGF-A mRNA expression in U87 cells; *C,* secretion of VEGF-A proteins by A549/8 cells; *D,* secretion of VEGF-A proteins by U87 cells. See also Supplementary Fig. S5.

UPR rather than the hypoxia-dependent response. This was based on the facts that (*a*) hypoxia is predictably reduced in this model because of the limited thickness of tumors and of their direct exposure to the air atmosphere, and (*b*) nutrient supply is limited to the CAM side of the tumors. Wild-type A549/8 cells, IRE1 DN cells, or cells transfected with the corresponding empty vector were deposited onto the CAM and grown up for 7 days (Fig. 4*A*). Under these conditions, solid tumors were readily observed at day 3 and slowly developed up to day 7. Histologic examination did not allow us to conclude about any significant differences in IRE DN cell– and pcDNA3 cell–derived tumors, except for the neovascularization process (Fig. 4*B* and *C*). A low number of blood vessels was observed in all tumor types at day 3 with a mean value of ~15 vessels/mm^2. Pericytes were not detected at this time in tumor tissues (not shown). The number of vessels then progressively increased with the number of pericytes at days 5 and 7 for the three types of tumors. However, a significantly lower number of vessels was observed in A549/8 IRE1 DN cell–derived tumors compared with tumors derived from control cells (Fig. 4*C*). These data suggest that IRE1 signaling contributes to tumor vascularization. The expression of the transcripts encoding VEGF-A, BiP, CHOP, HK-2, and PFKFB3 was also assessed by quantitative RT-PCR in tumors derived from IRE1 DN cells and pcDNA cells (Supplementary Fig. S6). A basal expression of VEGF-A mRNA was observed at day 0 of cell deposition onto the CAM. As expected, a slight increase of VEGF-A expression was observed at day 3, reached an ~3-fold maximum amplification at day 5, and then decreased at day 7 in tumors derived from pcDNA cells. The decrease of VEGF-A mRNA at day 7 in these tumors may depend on decreased cell viability observed in some tumor microenvironments at this stage of development, or on the down-regulation of its expression occurring at maximal angiogenesis. In IRE1 DN cell–derived tumors, VEGF-A up-regulation was delayed until day 7 (Supplementary Fig. S6). In addition, in both types of tumor, BiP and CHOP mRNA expression increased at days 3 and 5, the up-regulation of BiP mRNA being sustained at day 7, whereas that of CHOP mRNA decreased at this time. This suggests that the activation of UPR-related pathways are not exclusively dependent on IRE1. Finally, no significant increase in the expression of the two HIF-1–regulated genes *HK-2* and *PFKFB3* was observed, *PFKFB3* mRNA being even down-regulated in both tumor types (Supplementary Fig. S6). These data therefore show a significant correlation between the up-regulation of VEGF-A mRNA and the appearance of blood vessels in tumors. In addition, the up-regulation of VEGF-A mRNA in the two types of tumors paralleled that of mRNA encoded by known UPR target genes but not that of HIF-1 target genes. Our results therefore suggest a prevalence of ER stress–dependent signaling over HIF-1–regulated pathways in the CAM model.

We then tested the effect of the expression of IRE1 DN in an *in vivo* orthotopic model in which VEGF-A activity was reported to represent a major determinant of tumor progression (36). U87 pcDNA3 cells and U87 IRE1.NCK cells (two sets of independent clones of each) were implanted intracranially either in Rag γ mice (Fig. 5) or in nude mice (Supplementary Fig. S8) in two independent sets of experiments. The comparison of proliferation rates and phenotypes in culture, as well as growth in soft agar of several clones of stably transfected U87 (pcDNA3 and IRE1 DN) cells, is reported in Supplementary Fig. S7. Twenty-eight or 30 days postimplantation, brains were collected and snap frozen before serial sectioning. Significant phenotypic differences were observed between tumors (Fig. 5*A*). Indeed, tumors derived from pcDNA3-transfected cells were massive with well-delimited perimeters. A high cellularity was observed as well as an elevated microvascular density with the presence of tortuous blood vessels. In contrast, IRE1 DN cell–derived tumors were much smaller and exhibited stellate contours with extensive tumor cell infiltrations in the surrounding normal tissues. These tumors were also less vascularized than pcDNA3 cell–derived tumors, but occasionally presented hotspots of high vessel density in the periphery, at the close interface with normal tissues. These blood vessels exhibited features of telangiectatic vessels or of glomeruloid bodies. Necrosis was not significantly observed in control- and in DN-derived tumors. Tumors that developed after implantation of pcDNA3 cells ranged from 6 to 12 mm^3 in volume, whereas those obtained from DN-derived cells had significantly smaller volumes (average of ~1.7 mm^3; Fig. 5*B*). In addition, vessel density was ~2.3-fold lower in IRE1 DN cell–derived tumors than in pcDNA3 cell–derived tumors (Fig. 5*C*; see also Supplementary Fig. S8). These observations are consistent with the fact that angiogenesis and invasion are interdependent (37). The results established a correlation between an impaired IRE1 signaling and the decrease of tumor vascularization and growth.

Discussion

Angiogenesis represents a critical step in tumor development and is functionally linked to ischemia parameters, including hypoxia and glucose deprivation (1, 5, 38). Hypoxia-dependent intracellular signaling cascade involves the up-regulation of the HIF-1α transcription factor and is associated to tumor growth

through the activation of a number of genes regulating angiogenesis, cancer cell proliferation, and survival (1). In particular, HIF-1–dependent pathways lead to the up-regulation of the angiogenic growth factor VEGF-A mRNA after binding of HIF-1 on the HRE sequence located on the VEGF-A promoter (19, 20). Glucose deprivation, another stress whose occurrence has been reported in tumors (39–41), also induces VEGF-A up-regulation in normal and tumor cells in culture (15, 34, 42). Although glucose deprivation has been suggested to increase VEGF-A expression via HIF-1–related signaling (23–25), evidences for HIF-1–independent pathways have also been reported (17, 21, 22). Overall, the relationships between the responses of tumor cells to hypoxia and to glucose deprivation remain poorly understood.

In eukaryotes, the response to hypoxia and to glucose deprivation has been linked to ER-dependent signaling through the accumulation of incorrectly folded proteins within this compartment (35). Under those circumstances, an adaptive response named the UPR tends to restore ER and cell homeostasis disrupted by metabolic imbalances. At least two distinct components of the UPR are involved in the response of tumor cells to hypoxia. PERK activation has been identified as a major factor in hypoxia-mediated inhibition of translation in HeLa cells (9) and shown to play a role in tumor development (10). XBP1 was also shown to be essential for MEF-derived tumor growth *in vivo* and this effect was independent of the up-regulation of VEGF-A and fibroblast growth factor-2 (13). An integrated regulatory role of the UPR in tumor development was proposed by Ma and Hendershot (5).

In an attempt to assess the role of the UPR in ischemia-mediated tumor growth, we sought to analyze tumor cells responsiveness to hypoxia and/or to glucose deprivation. To this end, we evaluated the effect of IRE1 activation on the up-regulation of the angiogenic growth factor VEGF-A expression and on tumor growth and vascularization. We show that both hypoxia and glucose deprivation mediate the up-regulation of VEGF-A expression through IRE1 signaling in four different cellular models. Indeed, A549/8, U87 and C6 tumor cells expressing IRE1 DN transgenes significantly lose their ability to respond to these stresses by increasing VEGF-A expression. As compared with wild-type MEFs, *IRE1α*-null cells were also unable to increase the expression of VEGF-A mRNA upon low oxygen or low glucose culture conditions.

Our results therefore establish a functional link between IRE1 activity and VEGF-A up-regulation. Two intrinsic catalytic domains that exhibit Ser/Thr kinase and ribonucleolytic activities, respectively, are integral part of the IRE1 cytoplasmic moiety. A reported consequence of the ribonucleolytic activation of IRE1 is the unconventional splicing of XBP1 mRNA, which raises the question of the possible implication of XBP1 on VEGF-A expression. Previous reports have shown that the loss of XBP1 has little effect on the expression of the angiogenic growth factor in MEF cells (13). Besides, IRE1-mediated pathways independent of XBP1 may also be activated as shown by the fact that *ire-1* and *Xbp1* genes direct the expression of nonoverlapping sets of genes in *Caenorhabditis elegans* (43). In addition, a recent report indicated that IRE1 RNase controls the half-life of a significant number of mRNA in

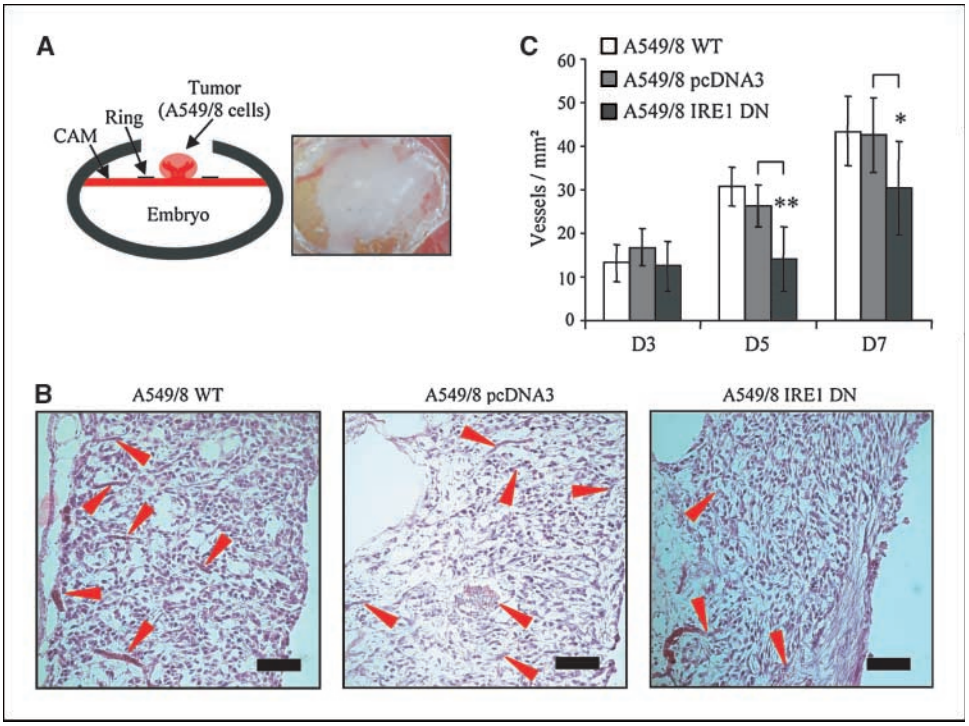

Figure 4. VEGF-A up-regulation and angiogenesis in IRE1 DN cell-derived tumors grown in the CAM assay. Wild-type A549/8 cells (*A549/8 WT*) or cells expressing either the IRE1 dominant negative (*A549/8 IRE1 DN*) or the empty vector (*A549/8 pcDNA3*) were deposited onto the CAM of embryonated chicken eggs (30). Solid tumors were then grown and removed from the CAM at days 3, 5, or 7. IRE1 DN (A549/8) cell–derived tumors still expressed IRE1.NCK at day 7 (Supplementary Fig. S4*B*). *A,* diagram of the chicken egg-CAM model (*left*) and above view (*right*) of a representative A549/8 cell–derived tumor after 5 d of development. *B,* histologic views of A549/8 cell–derived tumors at day 5. The presence of nucleated chick erythrocytes, of the blood vessel lining, and of the red labeling are indicative of the presence of tumor capillaries (*arrowheads*). SNA-1 lectin coupled to FITC and antibodies against human VEGF-R2 coupled to rhodamine were tentatively used for the detection of blood vessels. However, both markers were expressed on the surface of A549/8 cells and tissue discrimination was therefore not possible. *Bar,* 100 μm. *C,* quantification of blood vessel density at days 3, 5, and 7 was obtained by counting from 7 to 17 different fields over three to five different cryosections. *Columns,* mean (**P* < 0.01, ***P* < 0.005); *bars,* SD (see also Supplementary Figure S6 for gene expression analyses).

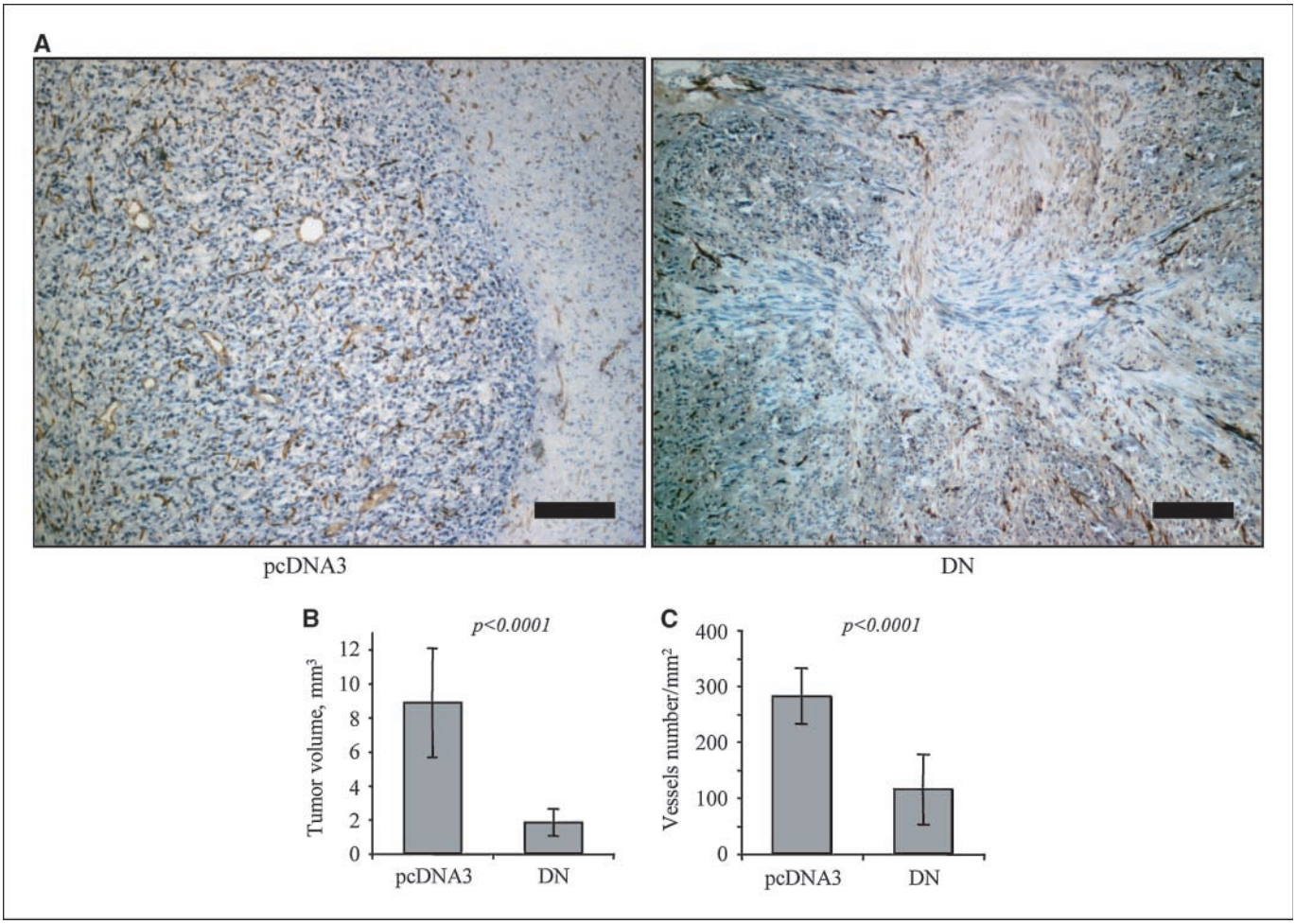

Figure 5. *In vivo* tumor development and angiogenesis in IRE1 DN cell–derived tumors developed in mouse brain. Intracranial implantation of U87 cells expressing either the IRE1 dominant negative (U87 IRE1 DN; clones 1C5 and 2A4) or the empty vector (U87 pcDNA3; clones T1P5 and T2P4) was done in Rag γ mice. Tumor development and capillary density were observed 28 d after injection. At this time, U87 IRE1 DN cells explanted from mice brain still expressed IRE1.NCK and retained a significant ability to inhibit XBP1 mRNA splicing (Supplementary Fig. S4*C*). *A,* histologic aspect of tumor sections. Immunohistochemical staining of endothelium was done according to standard methods using anti-CD31 antibodies. Sections were then counterstained using hematoxylin. Four to six tumors for each clone were analyzed and representative pictures are shown. *Bar,* 200 μm. *B,* measure of intracerebral tumor volume was determined and cumulated results are reported for the T1P5 and T2P4 control clones as well as for the 1C5 and 2A4 DN clones. Six independent tumors were measured for each clone. *Columns,* tumor volume average; *bars,* SD. The Student *t* test *P* value was determined ($P < 0.0001$). *C,* capillary number was counted by two independent investigators on a total of 46 (pcDNA3) and 68 (DN) sections for the two pairs of clones. The average vessel density was calculated as the ratio of vessel number per tumor section surfaces in mm^2. *Columns,* average; *bars,* SD. The Student's *t* test *P* value was determined ($P < 0.0001$). Similar experiments were done in nude mice using different pairs of U87 IRE1 DN and U87 pcDNA3 cell clones (Supplementary Fig. S8).

mammalian cells, including some whose translation products regulate angiogenic processes (44). Although other investigations are still necessary to address more precisely this question, our results obtained with C6 glioma cells expressing a nonfunctional mutant of the IRE1 kinase domain (K599A) indicated that the kinase activity is necessary to mediate the observed up-regulation of VEGF-A mRNA under both hypoxia and hypoglycemia. Finally, our data (Supplementary material S9) show that a functional link between IRE1 signaling and HIF-1 may exist, as the expression of HIF-1 mRNA and protein is reduced when IRE1 signaling is impaired. In keeping with this result, the expression of Hsp90, whose function has been linked to the maintenance of HIF-1 mRNA and protein (45, 46), also decreases in IRE1 DN–expressing cells (data not shown). Overall, these data suggest that IRE1 activity may represent an upstream integrating signal that could diverge toward the hypoxia- and hypoglycemia-mediated cellular responses and therefore affect tumor development.

Our results obtained *in vivo* support this hypothesis. Indeed, IRE1 DN (U87) cells developed smaller tumors than control cells in mouse brain although no major difference was observed between their respective proliferation rates in culture. In addition, IRE1 DN (U87) cell–derived tumors exhibited a reduced vascularization compared with their control counterpart, a result consistent with the delayed blood vessel appearance observed with IRE1 DN cells in the chicken CAM assay.

Because most of growing solid tumors is exposed to ischemic conditions in the first and avascular stage of their expansion, cancer cells are subjected to increased rate of genomic alterations. As a consequence, tumor cells progressively adapt and develop a higher tolerance to nutrient deprivation and hypoxia than normal cells (47–49). Part of this tolerance is associated to the constitutive or occasional activation of specific signaling pathways in such extreme conditions. The blockade of these rescuing events at key checkpoints therefore represents an interesting perspective for the selective inhibition of

tumor growth. Studies aiming to block HIF-dependent pathways have been developed as new approaches for cancer therapy (1). Besides, disruption of the UPR signaling may also provide an efficient way to sensitize tumor cells to their ischemic environment (48, 50). In this context, IRE1 appears as an interesting target that may limit the UPR signaling to reduce tumor cells adaptive potential.

Acknowledgments

Received 8/31/2006; revised 5/4/2007; accepted 5/11/2007.

Grant support: Ministère de la Recherche et de la Technologie, Institut National de la Santé et de la Recherche Médicale (INSERM), Ligue Nationale contre le Cancer, and Comité de la Gironde (M. Moenner); ARC grant 3694 (A. Bikfalvi); Canadian Institute for Health Research grant (E. Chevet); NIH grants HL052173 and DK42394 (R.J. Kaufman); International collaboration grant from the Fonds de la Recherche en Santé du Québec-INSERM; and Prix Institut Danone, alimentation et santé 2001 (B. Drogat). E. Chevet is a Fonds de la Recherche en Santé du Québec Junior scholar and R.J. Kaufman is an Investigator of the Howard Hughes Medical Institute.

The costs of publication of this article were defrayed in part by the payment of page charges. This article must therefore be hereby marked *advertisement* in accordance with 18 U.S.C. Section 1734 solely to indicate this fact.

We thank Dr. H. Esumi (Investigative Treatment Division, National Cancer Center Research Institute, Chiba, Kashiwa, Japan) for the gift of phVEGF1 and pSv-nlslacZ plasmids used for the gene reporter assays, Dr. J. Lang for allowing access to luminometer equipment, N. Allain-Courtois and F. Darlot for technical assistance with the immunohistochemistry, and X. Canron for help with endothelial cell assays.

References

1. Semenza GL. Targeting HIF-1 for cancer therapy. Nat Rev Cancer 2003;3:721–32.
2. Hardie DG. Minireview: the AMP-activated protein kinase cascade: the key sensor of cellular energy status. Endocrinology 2003;144:5179–83.
3. McMahon RJ, Frost SC. Nutrient control of GLUT1 processing and turnover in 3T3-1 adipocytes. J Biol Chem 1995;270:12094–9.
4. Spitz DR. Glucose deprivation-induced oxidative stress in human tumor cells. Ann N Y Acad Sci 2000; 899:349–62.
5. Ma Y, Hendershot LM. The role of the unfolded protein response in tumour development: friend or foe? Nat Rev Cancer 2004;4:966–77.
6. Kaufman RJ, Scheuner D, Schroder M, et al. The unfolded protein response in nutrient sensing and differentiation. Nat Rev Mol Cell Biol 2002;3:411–21.
7. Schroder M, Kaufman RJ. ER stress and the unfolded protein response. Mutat Res 2005;569:29–63.
8. Harding HP, Zhang Y, Ron D. Protein translation and folding are coupled by an endoplasmic-reticulum-resident kinase. Nature 1999;397:271–4.
9. Koumenis C, Naczki C, Koritzinsky M, et al. Regulation of protein synthesis by hypoxia via activation of the endoplasmic reticulum kinase PERK and phosphorylation of the translation initiation factor eIF2α. Mol Cell Biol 2002;22:7405–16.
10. Bi M, Naczki C, Koritzinsky M, et al. ER stress-regulated translation increases tolerance to extreme hypoxia and promotes tumor growth. EMBO J 2005;24: 3470–81.
11. Koritzinsky M, Magagnin MG, van den Beucken T, et al. Gene expression during acute and prolonged hypoxia is regulated by distinct mechanisms of translational control. EMBO J 2006;25:1114–25.
12. Yoshida H, Matsui T, Yamamoto A, Okada T, Mori K. XBP1 mRNA is induced by ATF6 and spliced by IRE1 in response to ER stress to produce a highly active transcription factor. Cell 2001;107:881–91.
13. Romero-Ramirez L, Cao H, Nelson D, et al. XBP1 is essential for survival under hypoxic conditions and is required for tumor growth. Cancer Res 2004;64:5943–7.
14. Ferrara N, Gerber HP, LeCouter J. The biology of VEGF and its receptors. Nat Med 2003;9:669–76.
15. Shweiki D, Neeman M, Itin A, Keshet E. Induction of vascular endothelial growth factor expression by hypoxia and by glucose deficiency in multicell spheroids: implications for tumor angiogenesis. Proc Natl Acad Sci U S A 1995;92:768–72.
16. Abcouwer SF, Marjon PL, Loper RK, Vander Jagt DL. Response of VEGF expression to amino acid deprivation and inducers of endoplasmic reticulum stress. Invest Ophthalmol Vis Sci 2002;43:2791–8.
17. Yun H, Lee M, Kim SS, Ha J. Glucose deprivation increases mRNA stability of vascular endothelial growth factor through activation of AMP-activated protein kinase in DU145 prostate carcinoma. J Biol Chem 2005;280:9963–72.
18. Chandel NS, Maltepe E, Goldwasser E, Mathieu CE, Simon MC, Schumacker PT. Mitochondrial reactive oxygen species trigger hypoxia-induced transcription. Proc Natl Acad Sci U S A 1998;95:11715–20.
19. Liu Y, Cox SR, Morita T, Kourembanas S. Hypoxia regulates vascular endothelial growth factor gene expression in endothelial cells. Identification of a 5′ enhancer. Circ Res 1995;77:638–43.
20. Forsythe JA, Jiang BH, Iyer NV, et al. Activation of vascular endothelial growth factor gene transcription by hypoxia-inducible factor 1. Mol Cell Biol 1996;16:4604–13.
21. Iyer NV, Kotch LE, Agani F, et al. Cellular and developmental control of O_2 homeostasis by hypoxia-inducible factor 1α. Genes Dev 1998;12:149–62.
22. Kotch LE, Iyer NV, Laughner E, Semenza GL. Defective vascularization of HIF-1α-null embryos is not associated with VEGF deficiency but with mesenchymal cell death. Dev Biol 1999;209:254–67.
23. Maltepe E, Schmidt JV, Baunoch D, Bradfield CA, Simon MC. Abnormal angiogenesis and responses to glucose and oxygen deprivation in mice lacking the protein ARNT. Nature 1997;386:403–7.
24. Carmeliet P, Dor Y, Herbert JM, et al. Role of HIF-1α in hypoxia-mediated apoptosis, cell proliferation and tumour angiogenesis. Nature 1998;394:485–90.
25. Ryan HE, Lo J, Johnson RS. HIF-1 α is required for solid tumor formation and embryonic vascularization. EMBO J 1998;17:3005–15.
26. Drogat B, Bouchecareilh M, North-Chassande S, et al. Acute L-glutamine deprivation compromises VEGF-A up-regulation in A549/8 cells. J Cell Physiol 2007;212: 463–72.
27. Nguyen DT, Kebache S, Fazel A, et al. Nck-dependent activation of extracellular signal-regulated kinase-1 and regulation of cell survival during endoplasmic reticulum stress. Mol Biol Cell 2004;15:4248–60.
28. Tirasophon W, Welihinda AA, Kaufman RJ. A stress response pathway from the endoplasmic reticulum to the nucleus requires a novel bifunctional protein kinase/endoribonuclease (Ire1p) in mammalian cells. Genes Dev 1998;12:1812–24.
29. Scheuner D, Song B, McEwen E, et al. Translational control is required for the unfolded protein response and *in vivo* glucose homeostasis. Mol Cell 2001;7: 1165–76.
30. Hagedorn M, Javerzat S, Gilges D, et al. Accessing key steps of human tumor progression *in vivo* by using an avian embryo model. Proc Natl Acad Sci U S A 2005;102: 1643–8.
31. Huang KC, Altinoz M, Wosik K, et al. Impact of the coxsackie and adenovirus receptor (CAR) on glioma cell growth and invasion: requirement for the C-terminal domain. Int J Cancer 2005;113:738–45.
32. Minchenko A, Leshchinsky I, Opentanova I, et al. Hypoxia-inducible factor-1-mediated expression of the 6-phosphofructo-2-kinase/fructose-2,6-bisphosphatase-3 (PFKFB3) gene. Its possible role in the Warburg effect. J Biol Chem 2002;277:6183–7.
33. Wertheimer E, Sasson S, Cerasi E, Ben-Neriah Y. The ubiquitous glucose transporter GLUT-1 belongs to the glucose-regulated protein family of stress-inducible proteins. Proc Natl Acad Sci U S A 1991;88:2525–9.
34. Iida K, Kawakami Y, Sone H, et al. Vascular endothelial growth factor gene expression in a retinal pigmented cell is up-regulated by glucose deprivation through 3′ UTR. Life Sci 2002;71:1607–14.
35. Kaufman RJ. Orchestrating the unfolded protein response in health and disease. J Clin Invest 2002;110: 1389–98.
36. Zilberberg L, Shinkaruk S, Lequin O, et al. Structure and inhibitory effects on angiogenesis and tumor development of a new vascular endothelial growth inhibitor. J Biol Chem 2003;278:35564–73.
37. Bello L, Giussani C, Carrabba G, Pluderi M, Costa F, Bikfalvi A. Angiogenesis and invasion in gliomas. Cancer Treat Res 2004;117:263–84.
38. Carmeliet P, Jain RK. Angiogenesis in cancer and other diseases. Nature 2000;407:249–57.
39. Vaupel P, Kallinowski F, Okunieff P. Blood flow, oxygen and nutrient supply, and metabolic microenvironment of human tumors: a review. Cancer Res 1989; 49:6449–65.
40. Ettinger SN, Poellmann CC, Wisniewski NA, et al. Urea as a recovery marker for quantitative assessment of tumor interstitial solutes with microdialysis. Cancer Res 2001;61:7964–70.
41. Ziegler A, von Kienlin M, Decorps M, Remy C. High glycolytic activity in rat glioma demonstrated *in vivo* by correlation peak 1H magnetic resonance imaging. Cancer Res 2001;61:5595–600.
42. Stein I, Neeman M, Shweiki D, Itin A, Keshet E. Stabilization of vascular endothelial growth factor mRNA by hypoxia and hypoglycemia and coregulation with other ischemia-induced genes. Mol Cell Biol 1995; 15:5363–8.
43. Shen X, Ellis RE, Sakaki K, Kaufman RJ. Genetic interactions due to constitutive and inducible gene regulation mediated by the unfolded protein response in C. elegans. PLoS Genet 2005;1:e37.
44. Hollien J, Weissman JS. Decay of endoplasmic reticulum-localized mRNAs during the unfolded protein response. Science 2006;313:104–7.
45. Isaacs JS, Jung YJ, Mimnaugh EG, Martinez A, Cuttitta F, Neckers LM. Hsp90 regulates a von Hippel Lindau-independent hypoxia-inducible factor-1 α-degradative pathway. J Biol Chem 2002;277:29936–44.
46. Minet E, Mottet D, Michel G, et al. Hypoxia-induced activation of HIF-1: role of HIF-1α-Hsp90 interaction. FEBS Lett 1999;460:251–6.
47. Izuishi K, Kato K, Ogura T, Kinoshita T, Esumi H. Remarkable tolerance of tumor cells to nutrient deprivation: possible new biochemical target for cancer therapy. Cancer Res 2000;60:6201–7.
48. Park HR, Tomida A, Sato S, et al. Effect on tumor cells of blocking survival response to glucose deprivation. J Natl Cancer Inst 2004;96:1300–10.
49. Lu J, Kunimoto S, Yamazaki Y, Kaminishi M, Esumi H. Kigamicin D, a novel anticancer agent based on a new anti-austerity strategy targeting cancer cells' tolerance to nutrient starvation. Cancer Sci 2004;95:547–52.
50. Blais J, Bell JC. Novel therapeutic target: the PERKs of inhibiting the integrated stress response. Cell Cycle 2006;5:2874–7.

IRE1 Signaling Is Essential for Ischemia-Induced Vascular Endothelial Growth Factor-A Expression and Contributes to Angiogenesis and Tumor Growth *In vivo*

Benjamin Drogat, Patrick Auguste, Duc Thang Nguyen, et al.

Cancer Res 2007;67:6700-6707.